machines

MDPI

Article

Synthesizing a Spatial Mechanism with a Hollow Core for Use in a Wrist Pronation and Supination Orthotic †

Tianze Xu [1], David H. Myszka [1], Clément Trotobas [2], Christine Azevedo [2] and Andrew P. Murray [1,*]

[1] Mechanical and Aerospace Engineering, University of Dayton, 300 College Park, Dayton, OH 45469, USA; xut004@udayton.edu (T.X.); dmyszka@udayton.edu (D.H.M.)
[2] Inria Centre d'Université Côte d'Azur, Université de Montpellier, 34095 Montpellier, France; clement.trotobas@gmail.com (C.T.); christine.azevedo@inria.fr (C.A.)
* Correspondence: murray@udayton.edu
† This paper is an extended version of our paper published in Trotobas, C.; Azevedo, C.; Murray, A.P. The Kinematic Synthesis of a Spherical Mechanism for Assisting in Wrist Pronation and Supination. In Proceedings of the 2023 ASME International Design Engineering Technical Conferences & Computers and Information in Engineering Conference (IDETC/CIE), ASME, Boston, MA, USA, 20–23 August 2023; Volume 8: 47th Mechanisms and Robotics Conference (MR). https://doi.org/10.1115/DETC2023-114766.

Abstract

Full use of the upper limb is necessary to carry out most tasks of daily life. Upper limb deficiencies, whether through complete or incomplete paralysis, inevitably lead to a loss of autonomy. Assistive orthoses are a potential method for restoring some autonomy. Pronation and supination, the turning of the wrist relative to the elbow, receives less focus than other joint movements in the arm. First, the utility of this degree-of-freedom in the arm is less obvious. Second, when compared to flexion and extension of the elbow, wrist prono-supination has no clear center of rotation due to the combined movement of the ulna and the radius bones as they cross and uncross in the forearm. This paper presents initial work in the design of a mechanism for a portable assistive orthosis that is expected to include powered prono-supination. The component proposed in this work is based on a spherical mechanism architecture. The capacity of these mechanisms to have a hollow center and to produce paths that follow arcs on spheres makes them worth consideration in this application. An optimization was carried out to perform path generation of a single spherical four-bar with the intent of replicating it three times to create the device proposed in this work. The mechanical design was modeled and a conceptual prototype was constructed to perform preliminary operational evaluations.

Keywords: linkage synthesis; spherical mechanism; wrist orthosis

check for updates

Academic Editor: Raffaele Di Gregorio

Received: 18 July 2025
Revised: 29 August 2025
Accepted: 5 September 2025
Published: 9 September 2025

Citation: Xu, T.; Myszka, D.H.; Trotobas, C.; Azevedo, C.; Murray, A.P. Synthesizing a Spatial Mechanism with a Hollow Core for Use in a Wrist Pronation and Supination Orthotic. *Machines* **2025**, *13*, 833. https://doi.org/10.3390/machines13090833

Copyright: © 2025 by the authors. Licensee MDPI, Basel, Switzerland. This article is an open access article distributed under the terms and conditions of the Creative Commons Attribution (CC BY) license (https://creativecommons.org/licenses/by/4.0/).

1. Introduction

Prono-supination, the rotation of the wrist relative to the elbow, allows for rotation of the hand to adjust grasp for tasks such as feeding or writing. This movement is beneficial for individuals with weak grasp as an object's weight can be shifted to the palm for better grip. The basic model of prono-supination movement is a gradual rotation from the elbow along the length of the forearm, producing motion at the wrist [1,2].

Limb deficiencies that impact autonomy reduce the capacity to perform activities of daily living and can require caregiver assistance [3,4]. Assistive orthoses are medical devices designed to support or assist the function of impaired limbs. Orthoses are typically worn externally and are customized to fit an individual's unique body structure and needs.

To optimize the functionality of a prono-supination orthosis, a rotation of the wrist relative to the elbow must be produced, with no components inside the forearm space, and with minimized size, power requirements, and weight. Multiple-degrees-of-freedom (*DOF*) wrist orthosis designs include those of Rocon et al. [5] and Dezman et al. [6].

The work presented in this paper investigates the use a low-degree-of-freedom assistive orthosis to uniquely address prono-supination, originally proposed in [7]. Low-*DOF* devices tend to have fewer components and, therefore, are more space-efficient and simpler in design. This simplicity can lead to increased reliability and reduced maintenance requirements. With fewer *DOF*, fewer actuators are required, with undemanding controls.

A spherical mechanism was selected for investigation into an assistive orthotic design for several reasons. First, a mechanism can be readily synthesized that is capable of producing complex motions [8]. Second, as their motion is prescribed by angles instead of lengths, spherical mechanisms can be designed to operate around a task, as seen in conceptualizations such as those in [9,10]. Third, spherical mechanisms have been considered in a variety of applications including the agile eye [11], wrists [12], assembly operations [13], grippers [14–16], and surgical robots [17]. Finally, the point of a path on the coupler of a spherical four-bar mechanism follows a trivariate quartic curve [18] that can designed to pass through exactly nine points [19] and above to satisfactory levels of accuracy [20,21]. This versatility of the spherical four-bar is used in this work to solve a 21 path point synthesis challenge.

In the orthotics available on the market and those being developed and tested in research, cable-driven systems are frequently employed due to their reliability, weight advantages, and their ability to perform extrinsic actuation. Implemented as external tendons, cables are commonly used as a means of transmission to drive machine components, such as links or pulleys. Since they are only capable of pulling, a pair of cables that work antagonistically are used. In a prono-supination orthosis, cables can vary the lengths of the rods to cause wrist rotation [6], or turn the wrist utilizing a C-shaped cuff along the forearm [22,23]. A pair of cables twisted around each other has been shown to produce high torques with low-speed movements [24]. Moreover, cables are frequently coupled with DC motors, providing significant weight and mobility advantages compared to pneumatic systems. As such, design decisions regarding the device under consideration in this paper are made to ensure it is conducive to being cable- and DC motor-driven.

This paper is organized as follows. In Section 2, the synthesis of a single four-bar mechanism to follow a trajectory that closely matches a constant line of latitude is presented. Section 3 details the kinematics of a spherical four-bar mechanism, focusing on the path of the coupler point meant to act as a critical spherical joint in the system design. Section 4 discusses the coupling of several of these mechanisms into a single mechanical system. The assembling and testing of a conceptual prototype is detailed in Section 5. Section 6 concludes the paper.

2. Synthesis of a Single Mechanism

The objective of the kinematic synthesis is to determine the dimensions of a spherical mechanism that directs a point on the coupler along a desired path. The desired path is specified by a set of path points that are placed on a sphere, along an 80° sweep on a constant line of latitude at 45° above the equator. These path points are shown as $\vec{P}_i$, $i = 1, \ldots, 21$, in Figure 1. The choice of 45° for the path points was derived from envisioning the prosthetic as a tube-like object to be placed around the forearm. With the fixed axes of the spherical mechanism located at −45°, the ends of the device can be observed on circles of the same size. Although any positive and negative angle of latitude provides such properties, the desire for the mechanism to be located on and move between the end circles

requires the circles to be away from the equator. Other angles of positive/negative latitude could be explored, but as the current goal was to validate the design concept, optimization was left for future work. The choice of the 80° sweep was derived from the goal sweep of 100° to encompass the range of prono-supination in most ADLs. Desirable sweep details are profiled in Section 4.4. With the design concept involving "stacked" components, as seen in the figure in Section 4.5, successfully achieving 80° was identified as the optimization goal.

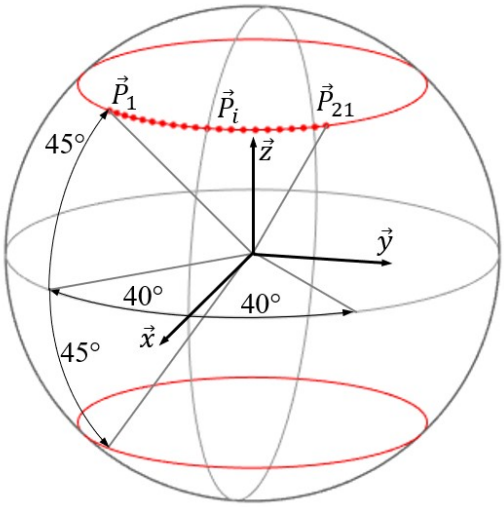


Figure 1. A coupler point on a spherical four-bar mechanism aiming to follow the path points $\vec{P}_i$ along the line of latitude 45° above the equator.

The position of the path points are given by

$$\vec{P}_i = \begin{bmatrix} P_{x_i} \\ P_{y_i} \\ P_{z_i} \end{bmatrix} = \begin{bmatrix} \cos 45^\circ \cos \phi_i \\ \cos 45^\circ \sin \phi_i \\ \sin 45^\circ \end{bmatrix} \tag{1}$$

where ϕ_i is 21 equally spaced values from $\phi_1 = -40^\circ$ to $\phi_{21} = 40^\circ$, using 4° increments. Note that the radius of the path points on the 45° circle of latitude is

$$r_P = \sqrt{P_{x_i}^2 + P_{y_i}^2} = \cos 45^\circ. \tag{2}$$

As a path synthesis problem with more than nine path points, an approximate motion optimization technique must be employed.

The fixed revolute joint axes of the spherical mechanism are designated $\vec{G}_1$ and $\vec{G}_2$, as shown in Figure 2. The moving revolute joint axes, corresponding with the ith position of the mechanism and specified in the fixed frame, are $\vec{Z}_{1,i}$ and $\vec{Z}_{2,i}$.

For these axes to define a spherical four-bar mechanism, the angles between the axes connected by each link must remain constant for all locations of the mechanism. Thus,

$$\cos \gamma = \vec{G}_1 \cdot \vec{G}_2, \tag{3}$$

$$\cos \alpha = \vec{G}_1 \cdot \vec{Z}_{1,i}, \tag{4}$$

$$\cos \beta = \vec{G}_2 \cdot \vec{Z}_{2,i}, \tag{5}$$

$$\cos \eta = \vec{Z}_{1,i} \cdot \vec{Z}_{2,i}, \tag{6}$$

where all vectors are assumed to be the same length as the unit. The remaining two angles that define the coupler are

$$\cos \eta_1 = \vec{Q}_i \cdot \vec{Z}_{1,i}, \tag{7}$$

$$\cos\eta_2 = \vec{Q}_i \cdot \vec{Z}_{2,i}. \tag{8}$$

The synthesis process seeks to obtain the values of γ, α, β, η, η_1, and η_2, such that the coupler point $\vec{Q}_i$ is located as close as possible to $\vec{P}_i$ as the mechanism moves.

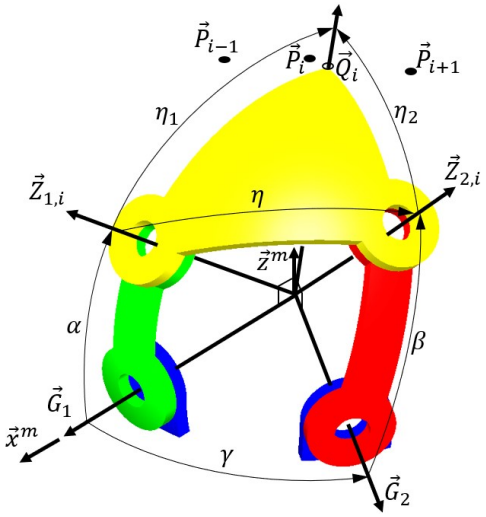


Figure 2. The axes of a spherical four-bar mechanism intersect at a common point.

Instead of determining the point $\vec{Q}_i$ as part of the optimization, its position is determined afterwards. This approach aims to minimize differences in the angles between the moving axes and the desired coupler point over the sweep of the mechanism. Thus,

$$J = \sum_{i=1}^{20} \left| \vec{P}_i \cdot \vec{Z}_{1,i} - \vec{P}_{i+1} \cdot \vec{Z}_{1,i+1} \right| + \left| \vec{P}_i \cdot \vec{Z}_{2,i} - \vec{P}_{i+1} \cdot \vec{Z}_{2,i+1} \right|. \tag{9}$$

Note the similarity of the terms in Equation (9) to those on the right side of Equations (7) and (8). For a mechanism that exactly reaches all of the $\vec{P}_i$, each term of Equation (9) would be $|\cos\eta_1 - \cos\eta_1| + |\cos\eta_2 - \cos\eta_2|$, resulting in $J = 0$. Using this approach, $\vec{Z}_{1,i}$ and $\vec{Z}_{2,i}$ for $i = 1, \ldots, 21$ are optimization variables. Several alternate optimization approaches could be considered. Many of the $\vec{Z}_{j,i}$ variables could be eliminated by introducing the position-dependent joint variables associated with loop closure, somewhat reducing the number of variables involved. Likewise, the coupler point location $\vec{Q}_i$ could also be explicitly introduced, adding another three variables per position and two location-dependent constraints per position, but allowing the optimization to be stated as minimizing the distance between $\vec{P}_i$ and $\vec{Q}_i$. Accurate and timely results were obtained via the proposed method, justifying its use and implementation in this design.

For equality constraints, Equations (3)–(6) were enforced over the range of i. Additionally, the requirement that all vectors are of unit length was introduced as a constraint. A desirable mechanism was deemed to be one with ring-like structures of the same size at both the $+45^\circ$ latitude circle for the coupler point and at the -45° latitude circle for the fixed pivots. As such, the z-components of $\vec{G}_1$ and $\vec{G}_2$ were constrained to $-\sin 45^\circ$ to keep them on the lower circle shown in Figure 1. The desired path points were constrained to one line of latitude, and the z-components of the fixed axes were limited to a different line of latitude because the intended use of the device requires that the vertical distance between the fixed axes and the coupler point remain (nearly) constant. Finally, as inequality constraints,

$$25^\circ \leq \alpha, \beta, \gamma, \eta \leq 90^\circ \tag{10}$$

were introduced for the sole purpose of constraining the mechanism to occupy a reasonable part of the surface area of the design sphere. The synthesis optimization can be formally stated as follows:

$$\begin{aligned}
&\underset{\vec{G}_1, \vec{G}_2, \vec{Z}_{1,i}, \vec{Z}_{2,i}}{\text{Minimize:}} && J, \quad i = 1, \ldots, 21 \\
&\text{subject to:} && \vec{G}_1 \cdot \vec{Z}_{1,j} - \vec{G}_1 \cdot \vec{Z}_{1,j+1} = 0, \quad j = 1, \ldots, 20 \\
& && \vec{G}_2 \cdot \vec{Z}_{2,j} - \vec{G}_2 \cdot \vec{Z}_{2,j+1} = 0, \\
& && \vec{Z}_{1,j} \cdot \vec{Z}_{2,j} - \vec{Z}_{1,j+1} \cdot \vec{Z}_{2,j+1} = 0. \\
& && \vec{G}_1 \cdot \begin{bmatrix} 0 & 0 & -1 \end{bmatrix}^T, \ \vec{G}_2 \cdot \begin{bmatrix} 0 & 0 & -1 \end{bmatrix}^T = \sin 45^\circ, \\
& && \vec{G}_1 \cdot \vec{G}_2, \ \vec{G}_1 \cdot \vec{Z}_{1,i}, \ \vec{G}_2 \cdot \vec{Z}_{2,i}, \ \vec{Z}_{1,i} \cdot \vec{Z}_{2,i} \leq \cos 90^\circ, \\
& && \cos 25^\circ \leq \vec{G}_1 \cdot \vec{G}_2, \ \vec{G}_1 \cdot \vec{Z}_{1,i}, \ \vec{G}_2 \cdot \vec{Z}_{2,i}, \ \vec{Z}_{1,i} \cdot \vec{Z}_{2,i}.
\end{aligned} \tag{11}$$

The `fmincon` function in MATLAB, v. R2022a, was employed for the optimization, using its default interior-point algorithm, along with the other default settings. The constraints were observed to be nonconvex.

The optimization produced values of $\alpha = 65.5^\circ$, $\beta = 65.7^\circ$, $\gamma = 61.3^\circ$ and $\eta = 64.2^\circ$. Other notable results of the optimization are listed in Table 1 and illustrated with the solid design model in Figure 3.

The final step of the synthesis is to determine η_1 and η_2 to complete the coupler and accurately locate the coupler point of the four-bar. This is achieved by averaging the angle found between the locations $\vec{P}_i$ and the corresponding moving axis locations $\vec{Z}_{1,i}$ and $\vec{Z}_{2,i}$, respectively, as follows:

$$\eta_1 = \cos^{-1}\left(\frac{\sum_{i=1}^{21} \vec{P}_i \cdot \vec{Z}_{1,i}}{21}\right), \tag{12}$$

$$\eta_2 = \cos^{-1}\left(\frac{\sum_{i=1}^{21} \vec{P}_i \cdot \vec{Z}_{2,i}}{21}\right). \tag{13}$$

These angles are calculated to be $\eta_1 = 81.7^\circ$ and $\eta_2 = 81.7^\circ$.

Table 1. The vectors defining the design of the spherical mechanism, determined via the optimization.

Vector	*x*-Component	*y*-Component	*z*-Component
$\vec{G}_1$	0.4933	−0.5066	−0.7071
$\vec{G}_2$	0.4863	0.5134	−0.7071
$\vec{Z}_{1,1}$	0.8936	0.3816	−0.2363
$\vec{Z}_{1,11}$	0.6723	0.5412	−0.5051
$\vec{Z}_{1,21}$	−0.2704	0.5634	0.5678
$\vec{Z}_{2,1}$	0.5677	−0.5631	−0.6005
$\vec{Z}_{2,11}$	0.7118	−0.5211	−0.4709
$\vec{Z}_{2,21}$	0.8946	−0.3767	−0.2404

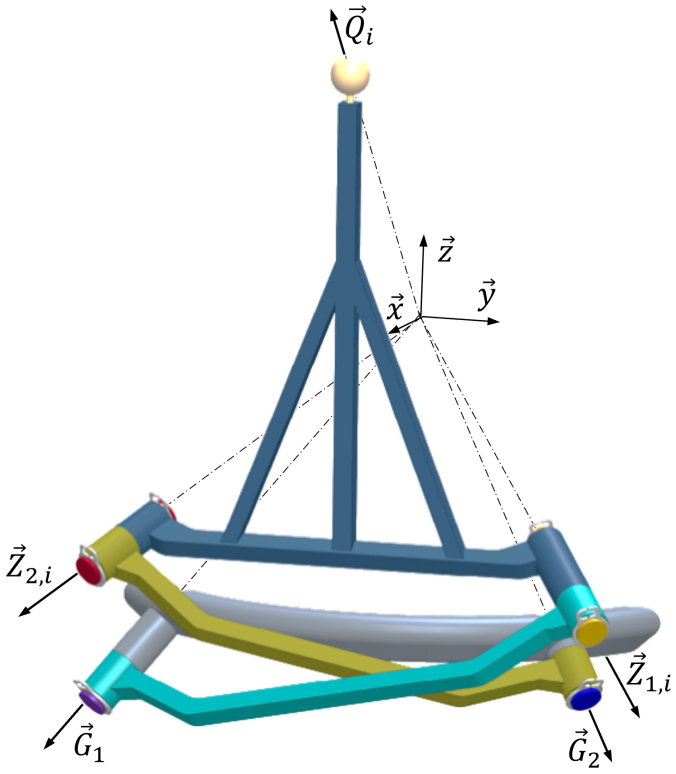


Figure 3. A solid model of the spherical mechanism optimization results.

3. Kinematics of a Single Mechanism

A kinematic model of the spherical mechanism that is synthesized in the previous section was constructed to assess the resulting motion characteristics. The notation provided in Figure 2 was used. The mechanism coordinate system was defined such that the x^m-axis is along $\vec{G}_1$ and the z^m-axis is along $\vec{G}_1 \times \vec{G}_2$. That is, $\vec{G}_1^m = [1, 0, 0]^T$. Rotation matrices are defined as follows:

$$\mathrm{R}_x(\theta) = \begin{bmatrix} 1 & 0 & 0 \\ 0 & \cos\theta & -\sin\theta \\ 0 & \sin\theta & \cos\theta \end{bmatrix}, \quad \mathrm{R}_z(\theta) = \begin{bmatrix} \cos\theta & -\sin\theta & 0 \\ \sin\theta & \cos\theta & 0 \\ 0 & 0 & 1 \end{bmatrix}.$$

The $\vec{G}_2^m$ axis is rotated at an angle γ from $\vec{G}_1^m$ that represents the fixed frame of the mechanism. Thus, $\vec{G}_2^m = \mathrm{R}_z(\gamma)\ \vec{G}_1^m = [\cos\gamma,\ \sin\gamma,\ 0]^T$. The $\vec{Z}_1^m$ axis is rotated at an angle α from $\vec{G}_1^m$, representing a pivoted link, and then rotated θ_1, representing the joint angle:

$$\vec{Z}_1^m = \mathrm{R}_x(\theta_1)\ \mathrm{R}_z(\alpha)\ \vec{G}_1^m = \begin{bmatrix} \cos\alpha \\ \sin\alpha\ \cos\theta_1 \\ \sin\alpha\ \sin\theta_1 \end{bmatrix}. \tag{14}$$

Likewise, the $\vec{Z}_2^m$ axis is rotated angle β from $\vec{G}_2^m$, representing the other pivoted link, and then rotated an angle θ_2, representing the joint angle:

$$\vec{Z}_2^m = \mathrm{R}_z(\gamma)\ \mathrm{R}_x(\theta_2)\ \mathrm{R}_z(\beta)\ \vec{G}_1^m = \begin{bmatrix} \cos\gamma\cos\beta - \sin\gamma\ \sin\beta\ \cos\theta_2 \\ \sin\gamma\cos\beta + \cos\gamma\ \sin\beta\ \cos\theta_2 \\ \sin\beta\ \sin\theta_2 \end{bmatrix}. \tag{15}$$

Substituting Equations (14) and (15) into Equation (6),

$$\begin{bmatrix} \cos\alpha \\ \sin\alpha\ \cos\theta_1 \\ \sin\alpha\ \sin\theta_1 \end{bmatrix} \cdot \begin{bmatrix} \cos\gamma\cos\beta - \sin\gamma\ \sin\beta\ \cos\theta_2 \\ \sin\gamma\cos\beta + \cos\gamma\ \sin\beta\ \cos\theta_2 \\ \sin\beta\ \sin\theta_2 \end{bmatrix} = \cos\eta. \tag{16}$$

Expanding Equation (16) leads to the following form:

$$A\ \cos\theta_2 + B\ \sin\theta_2 + C = 0, \tag{17}$$

where

$$\begin{aligned} A &= \sin\alpha\ \cos\gamma\ \sin\beta\ \cos\theta_1 - \cos\alpha\sin\gamma\sin\beta, \\ B &= \sin\alpha\ \sin\beta\ \sin\theta_1, \\ C &= \cos\alpha\ \cos\gamma\ \cos\beta + \sin\alpha\ \cos\theta_1\ \sin\gamma\ \cos\beta - \cos\eta. \end{aligned}$$

Using the widely known Method of the Auxiliary Angle [25], solving Equation (17) provides the relation between the drive joint angle θ_1 and driven joint angle θ_2,

$$\theta_2 = \tan^{-1}\left(\frac{B}{A}\right) \pm \cos^{-1}\left(\frac{-C}{\sqrt{A^2+B^2}}\right). \tag{18}$$

In summary, the motion of the spherical mechanism is parameterized by θ_1. Equation (18) is used to determine θ_2 which leads to and $\vec{Z}_1^m$ and $\vec{Z}_2^m$ from Equations (14) and (15), respectively. Further, Equations (7) and (8) are written in the mechanism coordinate system to solve for $\vec{Q}^m$, which is also parameterized by θ_1. The vectors $\vec{G}_1$ and $\vec{G}_2$ from Table 1 are used to construct a rotation matrix to transfer the coordinates from the mechanism reference frame (in Figure 2) to the orthotic reference frame (in Figure 1):

$$\begin{bmatrix} \vec{x} \\ \vec{y} \\ \vec{z} \end{bmatrix} = \begin{bmatrix} \vec{G}_1 & \dfrac{(\vec{G}_1 \times \vec{G}_2) \times \vec{G}_1}{\|(\vec{G}_1 \times \vec{G}_2) \times \vec{G}_1\|} & \dfrac{\vec{G}_1 \times \vec{G}_2}{\|\vec{G}_1 \times \vec{G}_2\|} \end{bmatrix} \begin{bmatrix} \vec{x}^m \\ \vec{y}^m \\ \vec{z}^m \end{bmatrix} = \mathrm{R}_m \begin{bmatrix} \vec{x}^m \\ \vec{y}^m \\ \vec{z}^m \end{bmatrix}. \tag{19}$$

The location of the coupler point $\vec{Q}$ in orthotic reference frame, as shown in Figure 3 is

$$\vec{Q} = \mathrm{R}_m\, \vec{Q}^m. \tag{20}$$

The angle that tracks the rotation of the coupler point $\vec{Q}$ relative to the orthotic z-axis is

$$\phi = \tan^{-1}\left(\frac{Q_x}{Q_y}\right), \tag{21}$$

where Q_x and Q_y and the x and y components of $\vec{Q}$.

The structural error is the difference between the specified path points $\vec{P}_i$ and point $\vec{Q}$ from Equation (20) as it sweeps throughout the range of motion $-40^\circ \leq \phi \leq 40^\circ$, which corresponds to $7.9^\circ \leq \theta_1 \leq 41.4^\circ$. Note that the synthesis was formulated on a unit sphere. For $\vec{P}_i$, $i = 1, \ldots, 21$, both the z-component and radius r_P are 0.7071. A motion curve of the synthesized linkage was created using θ_1 at 0.003° increments. The z-component of $\vec{Q}$ varies from 0.7037 to 0.7099, with a total variation of 0.0062. The radius of $\vec{Q}$ varies from 0.7042 to 0.7107, with a total variation of 0.0065. As stated earlier, a more sophisticated synthesis would involve significant algebraic manipulation to create an objective function that declares the mechanism dimensions as design variables. However, defining the moving axis vectors at each

of the precision points and using them as design variables permitted the rapid formulation of the optimization. The synthesis produced a realizable mechanism with low structural error.

4. Toward the Design of an Orthotic

The result of the optimization is a single spherical four-bar mechanism that includes a coupler point that tracks an 80° arc along the circle at 45° latitude. In this section, the implementation of this mechanism into the overall design is considered. As depicted in Figure 4, the mechanism is used three times, being rotated in its entirety by 120° around the central z-axis, located through the center of the rings. Three mechanisms are used to ensure stability of the top ring, akin to a tripod. The design of the bottom ring is observed as straightforward, as it simply constrains the fixed axes of the three individual four-bar mechanisms. The design of the top ring is seen to require additional considerations.

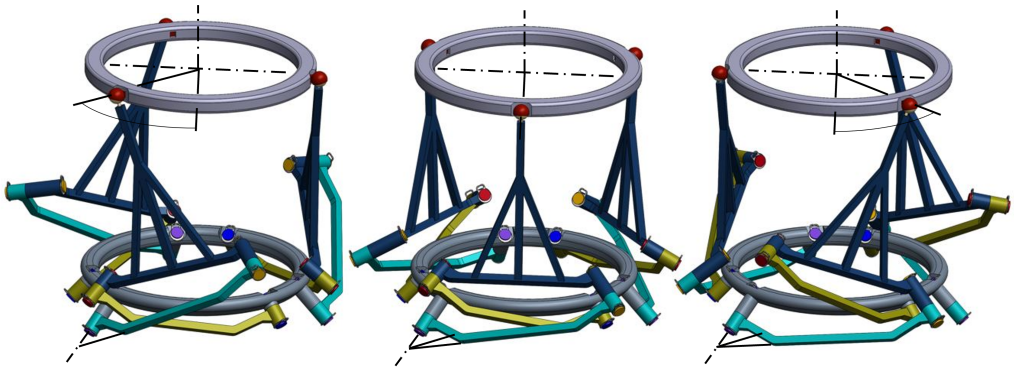


Figure 4. Solid models illustrating the general mechanical concept in three configurations.

The coupler point on each mechanism follows the same trajectory along a spherical path by rotating said trajectory by 120° about the central axis of the spherical device. As such, the distance between these points changes, even if the three four-bars are expected to move in unison. Connecting the three coupler points with a single part involves compensating for the structural error in both the radial and z directions. This combination of structural errors is addressed in the kinematic model through the inclusion of an S-joint and P-joint pair connecting the three coupler points to the ring. Here, to compensate for this structural error in the mechanical design, spherical joints are introduced at each coupler point with sufficient compliance to tolerate the minimal motion inward and outward from the center of the circle.

One additional observation about connecting the coupler points is warranted. Although the distance from a common circle center varies, if all three mechanisms move together, the angle from the circle center to any two of the coupler points stays constant at 120°. As such, the top ring is designed to constrain the axes of the three P joints to be separated by an angle of 120°.

4.1. Degrees of Freedom

A single spherical four-bar mechanism has one degree of freedom ($DOF = 1$). Uncoupled, three will have $DOF = 3$. The design proposes to couple the three four-bars, but in a way that does not require a strictly spherical architecture. The ball and prismatic joints allow the bodies to move without spheres that are concentric about the center point. Applying the standard spatial formalism to the proposed spherical device, the number of bodies is $L = 14$ including one fixed link, nine links in the three four-bars, three spherical joint-to-prismatic joint connections, and one coupling ring connecting the prismatic points. This leads to a total of 12 revolute (R) joints, 3 prismatic (P) joints, and 3 spherical (S) joints,

$$DOF = 6 \times (14 - 1) - 5 \times (15) - 3 \times (3) = -6. \tag{22}$$

This general spatial counting omits the idea that each spherical four-bar connects the R joints with intersecting axes, thereby creating a degree of freedom. A common approach for addressing this is to regard a spherical four-bar as a collection of one R joint with three cylindric (C) joints, changing nine joints from a single degree of freedom to two degrees of freedom:

$$DOF = 6 \times (13) - 5 \times (6) - 4 \times (9) - 3 \times (3) = 3. \quad (23)$$

Based on interactions with the solid model, three degrees of freedom for the spherical device appears to be correct.

To conclude that $DOF = 3$ is correct, the Fermat-Toricelli Point was considered. The F-T point is the unique point such that the sum of the distances from each of a triangle's three vertices to this unique point is minimized. In the case where the largest vertex angle of the triangle is $\leq 120^\circ$, this F-T point also views the three sides of the triangle at an angle of exactly 120°. This concept applies for three reasons. First, the top ring housing the 3 P joints was designed to require the joints to act along lines separated by an angle of 120°. Second, moving the four-bar mechanisms independently identifies three unique locations for the S joints in space. Finally, as each S joint only has a limited range of motion on the sphere, the triangle connecting the three points always has vertices forming angles of less than 120°. In conclusion, defining the locations of the S joint at each mechanism's coupler point independently, and introducing the requirement that the floating ring is used to separate the P joint axes by 120°, the spatial triangle obtains a unique F-T point. Thus, $DOF = 3$ is an appropriate conclusion for the overall spherical device, including the ring coupling the three four-bar mechanisms.

4.2. Reducing DOFs from Three to One

Although the spherical device as proposed has three *DOFs*, the additional motion capacity is not desirable when the intended use is prono-supination. The *DOFs* can be reduced through the observation that the three identical four-bar mechanism instances should all have identical coordinated actuation. As such, a single actuator mechanically connected to the three inputs reduces the *DOFs* from three to one. One mechanical design of the orthotic device is illustrated in Figure 5. The design involves a single cable actuation that rotates a spool within the frame. Bevel gear segments are formed within the spool that pair with a gear attached to one pivoted link on each of the three mechanisms. Thus, the input motion to the three identical mechanisms is coordinated to be identical.

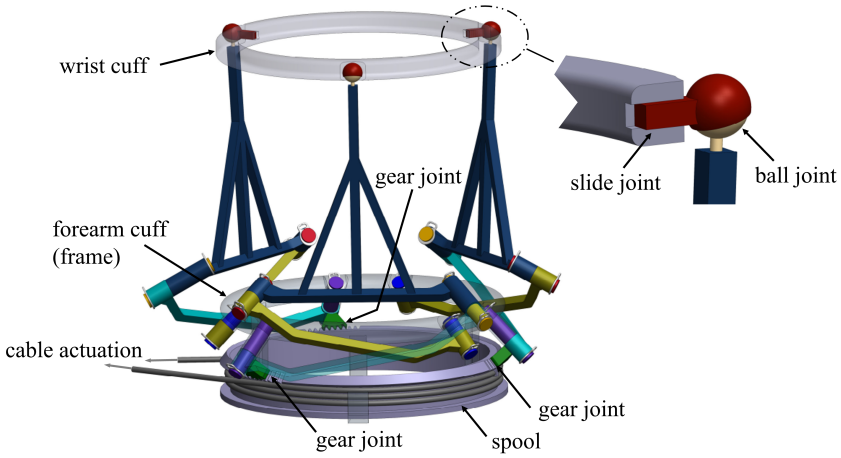


Figure 5. Three spool mounted gear joints will actuate one pivoted link (shown in cyan) on each of the three mechanisms.

4.3. Mechanical Advantage

Mechanical advantage MA is a measure of the effectiveness with which a machine amplifies an input force to perform its work. In the case of the proposed spherical device, this is defined as the ratio of the output torque produced by the machine to the input torque applied,

$$MA = \frac{T_\phi}{T_{\theta_1}}. \tag{24}$$

An $MA < 1$ means the device amplifies displacement, requiring a shorter actuator stroke, although at the cost of requiring a greater force. A low MA is associated with motion amplification and lends well to actuation, as proposed in Figure 5, thereby reducing the length of cable moving from the spool.

The instantaneous velocity ratio through the device is the ratio of the output rotational speed ($\dot{\phi} = d\phi/dt$) to the input rotational speed ($\dot{\theta}_1 = d\theta_1/dt$). Thus,

$$VR = \frac{d\phi/dt}{d\theta_1/dt} = \lim_{\Delta\theta_1 \to 0} \frac{\Delta\phi}{\Delta\theta_1}. \tag{25}$$

Equations (17)–(21) are used to determine ϕ at small increments of θ_1. With those values, a series of instantaneous VR are predicted using Equation (25). Assuming energy is conserved through the device,

$$T_\phi \, \dot{\phi} = T_{\theta_1} \, \dot{\theta}_1, \tag{26}$$

which concludes that

$$MA = \frac{1}{VR} = \lim_{\Delta\theta_1 \to 0} \frac{\Delta\theta_1}{\Delta\phi}. \tag{27}$$

Therefore, the instantaneous mechanical advantage of the device is readily determined from the kinematic model.

4.4. Review of Orthosis Requirements

To consider this device as a component in prono-supination orthosis, such as the partial concept in Figure 6, some technical requirements for ADL assistance are considered. One study produced maximum pronation and supination torques of 13.0 Nm and 14.8 Nm respectively [26]. However, another study found the maximum torque in some individuals to be as low as 3.33 Nm for pronation and 3.08 Nm for supination [27]. The observed differences in torque values are attributed to variations in study participants and protocols, such as variations in the participants' gender or dominant hand, the position of the forearm, and the position of the elbow joint. The range of motion for pronation and supination, respectively, varies from 77.23° to 81.2° and from 82.4° to 93.13° from the neutral position, i.e. hand-shake position, depending on age, gender, and measurement method [28,29]. Additionally, the median maximal velocities for supination and pronation were found to be 428° per second and 406° per second, respectively, depending on gender, dominant hand, and position of the elbow [30].

The prono-supination movement primarily serves to position the hand, noting that the maximal torque, range of motion, and velocity are not needed to achieve ADLs. An investigation of 19 ADLs determined that the maximum required torque for supination was 0.06 Nm, with less than 0.05 Nm being required for pronation [4]. An earlier study revealed that only 100° of forearm rotation was needed for ADLs [31], with an 80° range of motion, from 30° supination to 50° pronation, covering seven of the eight ADLs studied. Although certain tasks may require significant pronation or supination, recent research indicates that the maximum displacement arc of prono-supination in an ADL is 103 ± 34°, observed when using a fork [32]. According to this study, an appropriately positioned

80° range would mostly or completely address seven ADLS, partially contribute to three, and would not contribute to the remaining one. One study goes so far as to suggest that the arm is so adaptive that its specific motions during tasks is less important to understand than the start and end points for the task [3]. The mechanism developed in Section 4 was designed to produce a limited range of motion at 80°. Although some ADLs lie within this range, it is insufficient for accomplishing all ADLs. Table 2 shows the range of motion, torque, mass, and actuation schemes of several prono-supination orthoses.

Table 2. Characteristics of prono-supination orthoses found in the literature.

Reference	Motion	Torque	Actuation
Realmuto [33]	95°	1.5 Nm	Pneumatic, fabric based
Bartlett [34]	78°	0.5 Nm	Pneumatic, McKibben
Dežman [6]	180°	N/A	DC motor, cable and rod
Dias [22]	150°	N/A	DC motor and bowden cable
Buongiorno [23]	146°	6.3 Nm	DC motor and cable
Tsabedze [24]	118°	N/A	DC motor and twisted cable

4.5. Generating an Orthosis from the Spherical Device

A single spherical mechanism, resulting from the synthesis provided herein, moves comparably to the first two devices listed in Table 2. The orthotic concept can be extended by stacking two such devices, keeping the outer radius of the orthotic only modestly larger than the arm. The two layers would include three rings, as shown in Figure 6. One ring would be at the proximal end of the forearm, attached near the elbow, one at the distal end, connected to the wrist, and one between them and not attached to the forearm. The idea of stacking two such devices doubles the achievable range of motion to 160°, well beyond the 100° specified for ADLs. The top device is expected to be driven mechanically through a connection to the bottom device, keeping the *DOF* of the system at one, but could be actuated independently as well. This raises the need to design the original mechanism to simply achieve the required 100° sweep. The device was designed to achieve only 80° of motion because an increase results in the coupler point traveling a greater distance along z, especially given the other constraints on the design.

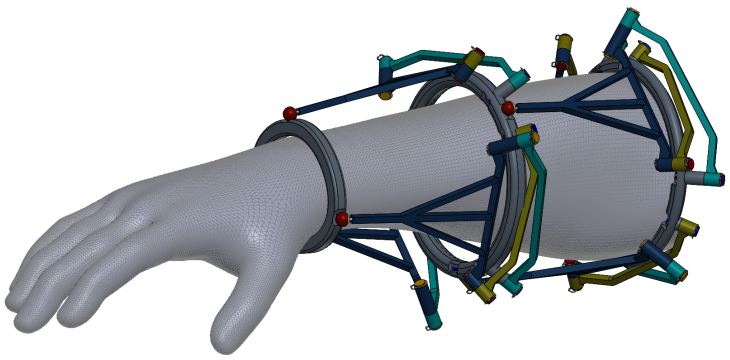


Figure 6. The design concept under consideration stacks the proposed device to extend from being adjacent to the elbow to become in line with the wrist.

5. Device Prototype and Evaluation

Proof-of-concept prototypes of the device generated in the prior section were constructed to confirm the range of motion, degrees of freedom, and transmission of loads. One version is shown in Figure 7, where the actuated pivot links, the driven pivoted links, and

couplers are printed in pink, green and blue, respectively. This prototype was produced with a Bambu Lab (Shenzhen, China) A1 Mini printer. A nozzle size of 0.2 mm was used. The material is PLA, with a minimum elastic modulus of 2000 MPa and tensile strength of 31 MPa. The spherical mechanisms were scaled such that the inner diameter of the top ring was 60 mm. To achieve an acceptable operational fit within the revolute joints, the holes in the printed links were resized with a hand reamer and steel pins were inserted. White printed end caps were pressed onto the pins, as can be seen in Figure 7. Three ball joints joined the couplers to the top ring to serve as the orthotic wrist attachment. Those ball joints provide sufficient compliance to absorb the small structural errors in the synthesized mechanism. The ball joints on a functional orthosis would likely be produced from a turned aluminum ball and a socket molded from bearing-grade polymers. Additionally, the section size and material choice for the links would be optimized to balance rigidity and weight. The mechanical design details of the links and joint clearances that provide minimal freeplay remain for future work.



Figure 7. A concept prototype of the orthotic mechanism.

In a second prototype [7], a single actuator was connected via cables and pulleys to the three actuated mechanism links and produced the desired motion of the top ring. That prototype successfully demonstrated that the input *DOFs* could be reduced to one.

A fixture was constructed to secure the prototype shown in Figure 7 to perform preliminary evaluations of its motion and force transmission characteristics. The prototype inserted within the fixture and configured for force transmission testing is presented in Figure 8. The fixture involves a pair of concentric tubes, separated by a small clearance (1.0 mm) and coated with a solid lubricant to allow for low-friction relative rotation. The frame of the device was clamped to a flange on the outer tube. The flange of the outer tube fits within a base that is clamped to a work surface. The top ring of the device is clamped to a flange on the inner tube. Thus, the angle of the top ring on the device can be precisely positioned and the configuration of the three mechanisms is coordinated.

The fixture includes graduations to measure θ_1 and ϕ. A motion test protocol was composed that located the actuated pivoted link within its operating range of $-40^\circ \leq \phi \leq 40^\circ$. At each set position, θ_1 was measured. A plot of θ_1 vs. ϕ, derived from Equation (21), is shown in Figure 9a as the solid curve. The experimental evaluation of the prototype is shown via circular markers. The close match between the kinematic model and testing

confirms the synthesis optimization results and the accuracy of the linkage parameters and joint construction.

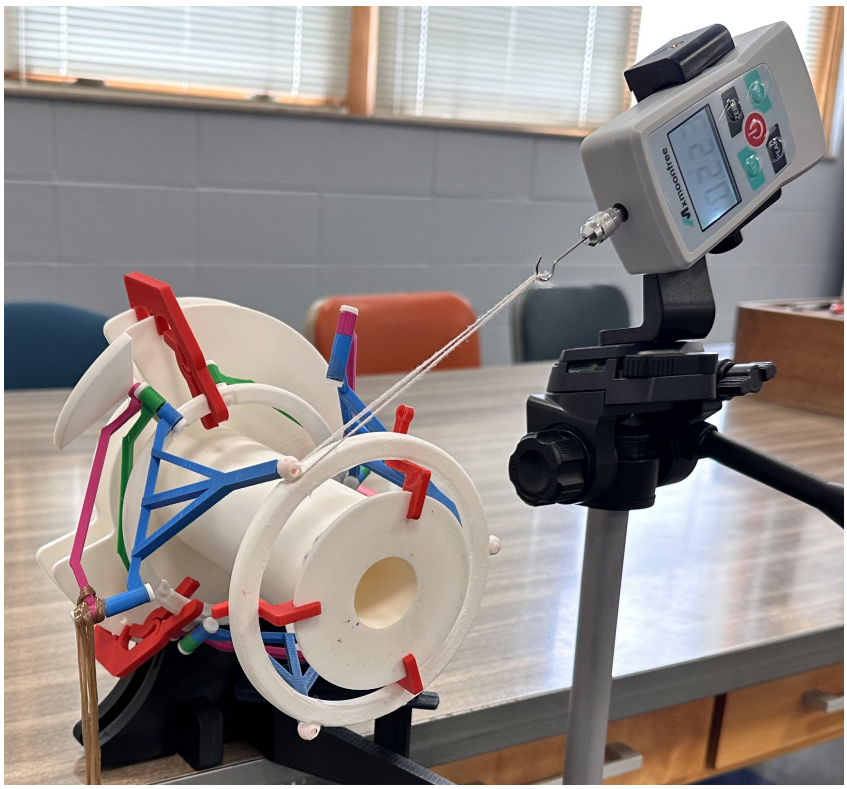
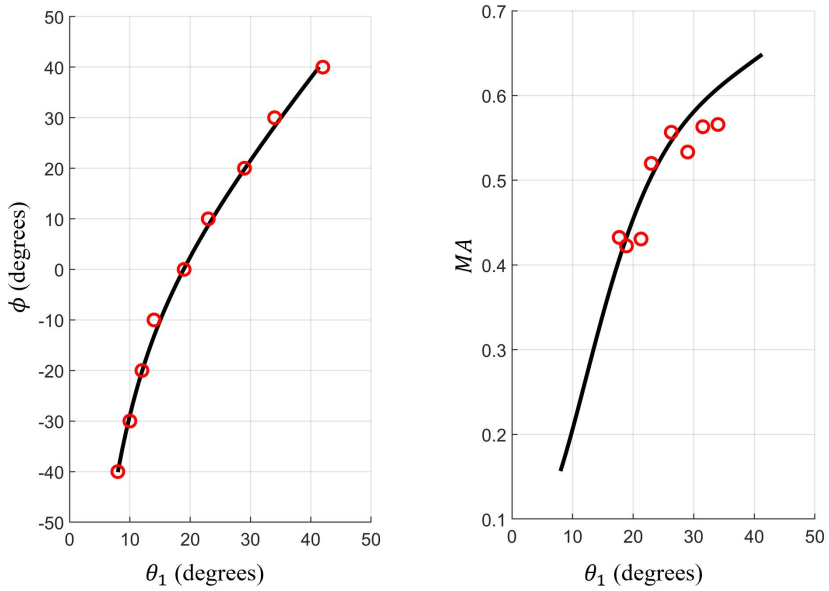


Figure 8. The device was placed within a fixture to evaluate the range of motion and load transmission.



(**a**) Device motion (**b**) Mechanical advantage

Figure 9. Results from the synthesis model (solid curves) and prototype evaluations (circle markers), (**a**) validating the kinematics, and (**b**) validating the load characteristics.

A force transmission test protocol was formulated that similarly set a mechanism configuration by precisely locating the top ring. At each set position, a weight W was hung from the moving end of one of the actuated links. The hanging weight produces a torque at the actuated joint of $\vec{T}_1^m = r_1 \times W\ \vec{g}$, where r_1 is the vector from $\vec{G}_1$ to $\vec{Z}_{1_i}$ at the radius of

the actuated link and $\vec{g} = [-0.4330,\ 0.5066,\ 0]^T$ is a unit vector representing the direction of gravity transformed for reorienting the device into the fixture. The torque on the actuated pivot axis T_{θ_1} is the third component of $\vec{T}_1$. A force gauge was positioned with a cord to restrain the motion of the top ring. Care was taken to position the cord tangentially to the ring, as seen in Figure 8. Thus, the restraining torque was $T_\phi = r_r\, F_g$, where r_r is the radius of the top ring and F_g is the force measured on the gauge. The test range was limited to $-3^\circ \leq \phi \leq 28^\circ$ due to interference between the hanging weight and the other links.

To determine the MA at a specific mechanism configuration, various values of W were applied and the corresponding value of F_g was measured. A plot of T_ϕ vs. T_{θ_1} for each W was generated, where the slope of the straight line through those points represented MA. The intercept of the straight line represented the friction within the joints, and was ignored. A plot of θ_1 vs. MA from Equation (27) is shown in Figure 9b as a solid curve. The experimental evaluation values of MA from the prototype are shown as circular markers. The experiments illustrate the expected trend; however, friction resulted in appreciable noise in the measurements.

The stated goal is for the orthotic to be cable-driven, as this is a common approach to orthotic design due to the ability of cable drivers to allow for actuators to be mounted a significant distance from the mechanism itself and their capacity to deliver reasonable loads from modestly sized actuators. A survey of orthotic design, especially those associated with the arm, reveals that cable drives are often used in applications of this sort. The survey in [35] details many designs of this type, some of which are listed in Table 2. The results of Figure 9 provide guidance on the selection of the force, maximum displacement, and speed requirements of an actuator for an orthotic device. The mechanical configuration shown in Figure 5 has a 4.5 gear joint ratio, a spool diameter of 72 mm, and cuff diameter of 60 mm (as does the prototye in Figure 8). Achieving a full range of $\Delta\phi = 80^\circ$ requires $\Delta\theta_1 = 35^\circ$, as observed in Figure 9a. Considering the gear ratio of 4.5, the full range spool rotation is 8°. With a spool diameter of 72 mm, a cable pull of 5 mm is required between extreme positions. The twisted string actuators (TSAs) used in the work of Tsabedze et al. [24] offer a lightweight solution for such low-displacement and high-torque applications. Small-scale TSAs can produce up to 50 N force [24]. The mechanism configuration with the worst mechanical advantage ($\theta_1 = 8^\circ$) has $MA = 0.17$, as observed in Figure 9b. Again, considering the gear ratio and spool diameter, a 50 N actuator force would provide a spool torque of 1.8 Nm and a wrist torque of 0.07 Nm, which is sufficient for the 19 ADLs identified in Perry et al. [4].

6. Conclusions

The focus of this work was on the kinematic synthesis of a mechanism that could be used in a prono-supination orthotic. First, a spherical four-bar mechanism was synthesized to allow for the rotation of a ring component that stays close to a 45° line of latitude. Second, three of these four-bar mechanisms were combined into a single device. This device, being able to create an 80° range of motion at the top ring relative to the bottom ring while holding the top ring at a nearly fixed distance from the bottom ring, shows promising motion properties in this application. To accomplish all ADLs, an additional 20° of motion is necessary. One proposal for accomplishing this, providing the wrist with something akin to its full range of motion, would be to stack two of these devices end-to-end.

This work also evaluated the proposed concept in terms of the state of the art in orthotic design and the corresponding biomechanical requirements. Portability imposes many design requirements that are difficult for any individual design to address. Intriguingly, for this specific part of a more complex arm orthotic, the torque requirements for assisting in ADLs are exceedingly low, at 0.06 Nm. Thus, this part of the orthotic can focus on comfort,

usability, developing the kinematics of the motion, and minimizing the encumbrance of the system, as opposed to focusing on the powering and actuation needs. This paper presented some of the initial investigation into these topics. As such, this work does not encompass many of the facets of an assistive arm orthosis, and the feasibility of the mechanism as a prono-supination component in an orthosis has yet to be demonstrated, remaining a subject for future work.

Author Contributions: Conceptualization, A.P.M., C.A., C.T. and D.H.M.; methodology, D.H.M., A.P.M. and C.T.; software, T.X. and A.P.M.; validation, C.T. and T.X.; formal analysis, T.X., D.H.M. and A.P.M.; investigation, T.X. and A.P.M.; resources, T.X.; data curation, C.T. and T.X.; writing—original draft preparation, C.T., D.H.M. and A.P.M.; writing—review and editing, T.X., D.H.M., A.P.M., C.T. and C.A.; visualization, T.X., D.H.M., A.P.M. and C.T.; supervision, D.H.M., A.P.M. and C.A.; project administration, D.H.M. and A.P.M. All authors have read and agreed to the published version of the manuscript.

Funding: The authors would like to thank The University of Montpellier's LabEx NUMEV (Digital and Hardware Solutions for the Environmental and Life Sciences) for their funding in support of this work. This work has also been supported in part by the University of Dayton Office for Graduate Academic Affairs through the Graduate Student Summer Fellowship Program.

Informed Consent Statement: Not applicable.

Data Availability Statement: Data is available upon request.

Acknowledgments: The authors would like to thank The University of Montpellier's LabEx NUMEV (Digital and Hardware Solutions for the Environmental and Life Sciences) for their funding in support of this work. We would like to thank the University of Dayton student Brad Becker for creating some of the solid models.

Conflicts of Interest: The authors declare no conflicts of interest.

References

1. Pennestrì, E.; Stefanelli, R.; Valentini, P.P.; Vita, L. Virtual Musculo-Skeletal Model for the Biomechanical Analysis of the Upper Limb. *J. Biomech.* **2007**, *40*, 1350–1361. [CrossRef] [PubMed]
2. Laitenberger, M.; Raison, M.; Périé, D.; Begon, M. Refinement of the Upper Limb Joint Kinematics and Dynamics Using a Subject-Specific Closed-Loop Forearm Model. *Multibody Syst. Dyn.* **2015**, *33*, 413–438. [CrossRef]
3. Buckley, M.A.; Yardley, A.; Johnson, G.R.; Cams, D.A. Dynamics of the Upper Limb during Performance of the Tasks of Everyday Living—A Review of the Current Knowledge Base. *Proc. Inst. Mech. Eng. Part H J. Eng. Med.* **1996**, *210*, 241–247. [CrossRef] [PubMed]
4. Perry, J.C.; Rosen, J.; Burns, S. Upper-Limb Powered Exoskeleton Design. *IEEE/ASME Trans. Mechatron.* **2007**, *12*, 408–417. [CrossRef]
5. Rocon, E.; Gallego, J.; Belda-Lois, J.; Benito-León, J.; Pons, J. Biomechanical Loading as an Alternative Treatment for Tremor: A Review of Two Approaches. *Tremor Other Hyperkinetic Mov.* **2012**, *2*, 1–13. [CrossRef]
6. Dežman, M.; Asfour, T.; Ude, A.; Gams, A. Exoskeleton Arm Pronation/Supination Assistance Mechanism With A Guided Double Rod System. In Proceedings of the 2019 IEEE-RAS 19th International Conference on Humanoid Robots (Humanoids), Toronto, ON, Canada, 15–17 October 2019; pp. 559–564.
7. Trotobas, C.; Azevedo, C.; Murray, A.P. The Kinematic Synthesis of a Spherical Mechanism for Assisting in Wrist Pronation and Supination. In Proceedings of the 47th Mechanisms and Robotics Conference (MR): 2023 ASME International Design Engineering Technical Conferences & Computers and Information in Engineering Conference (IDETC/CIE), ASME, Boston, MA, USA, 20–23 August 2023; Volume 8. [CrossRef]
8. McCarthy, J.M.; Soh, G.S. *Geometric Design of Linkages*; Springer: New York, NY, USA, 2010.
9. Larochelle, P.; Dooley, J.; Murray, A.; McCarthy, J.M. Sphinx: Software for Synthesizing Spherical 4r Mechanisms. In Proceedings of the NSF Design and Manufacturing Systems Conference, Charlotte, NC, USA, 6–8 January 1993; Volume 1, pp. 607–611.
10. Essomba, T.; Vu, L.N. Kinematic Analysis of a New Five-Bar Spherical Decoupled Mechanism with Two-Degrees of Freedom Remote Center of Motion. *Mech. Mach. Theory* **2018**, *119*, 184–197. [CrossRef]
11. Gosselin, C.M.; Hamel, J.F. The Agile Eye: A High-Performance Three-Degree-of-Freedom Camera-Orienting Device. In Proceedings of the 1994 IEEE International Conference on Robotics and Automation, San Diego, CA, USA, 8–13 May 1994; Volume 1, pp. 781–786. [CrossRef]

12. Hess-Coelho, T.A. A Redundant Parallel Spherical Linkage for Robotic Wrist Application. *J. Mech. Des.* **2007**, *129*, 891–895. [CrossRef]
13. Murray, A.; Pierrot, F. Design of High-Speed Spherical Four-Bar Mechanism for Use in a Motion Common in Assembly Processes. In Proceedings of the 2007 ASME Design Engineering Technical Conferences, Las Vegas, NV, USA, 4–7 September 2007.
14. Kocabas, H. Gripper Design with Spherical Parallelogram Linkage. *J. Mech. Des.* **2009**, *131*, 075001. [CrossRef]
15. Acar, O.; Saglam, H.; Şaka, Z. Evaluation of grasp capability of a gripper driven by optimal spherical mechanism. *Mech. Mach. Theory* **2021**, *166*, 104486. [CrossRef]
16. Patel, V.V.; Dollar, A.M. Robot hand based on a spherical parallel mechanism for within-hand rotations about a fixed point. In Proceedings of the 2021 IEEE/RSJ International Conference on Intelligent Robots and Systems (IROS), Prague, Czech Republic, 27 September–1 October 2021; pp. 709–716.
17. Wu, C.; Liu, X.J.; Wang, L.P.; Wang, J.S. Optimal Design of Spherical 5R Parallel Manipulators Considering the Motion/Force Transmissibility. *J. Mech. Des.* **2010**, *132*, 031002. [CrossRef]
18. Bai, S. Algebraic Coupler Curve of Spherical Four-Bar Linkages and Its Applications. *Mech. Mach. Theory* **2021**, *158*, 104218. [CrossRef]
19. Chiang, C.H. Synthesis of Spherical Four-Bar Path Generators. *Mech. Mach. Theory* **1986**, *21*, 135–143. [CrossRef]
20. Peñuñuri, F.; Peón-Escalante, R.; Villanueva, C.; Cruz-Villar, C.A. Synthesis of Spherical 4R Mechanism for Path Generation Using Differential Evolution. *Mech. Mach. Theory* **2012**, *57*, 62–70. [CrossRef]
21. Li, X.; Shi, A.; Feng, L.; Zhang, Y. A Novel Analytical Method for Path Synthesis of Spherical Four-Bar Mechanism Based on Fourier Series. In Proceedings of the 2024 6th International Conference on Reconfigurable Mechanisms and Robots (ReMAR), Chicago, IL, USA, 24–27 June 2024. [CrossRef]
22. Dias, E.A.; de Andrade, R. Design of a Cable-driven Actuator for Pronation and Supination of the Forearm to Integrate an Active Arm Orthosis. In Proceedings of the 1st International Electronic Conference on Actuator Technology: Materials, Devices and Applications, Online, 23–27 November 2020; p. 8511.
23. Buongiorno, D.; Sotgiu, E.; Leonardis, D.; Marcheschi, S.; Solazzi, M.; Frisoli, A. WRES: A Novel 3 DoF WRist ExoSkeleton With Tendon-Driven Differential Transmission for Neuro-Rehabilitation and Teleoperation. *IEEE Robot. Autom. Lett.* **2018**, *3*, 2152–2159. [CrossRef]
24. Tsabedze, T.; Hartman, E.; Brennan, C.; Zhang, J. A Compliant Robotic Wrist Orthosis Driven by Twisted String Actuators. In Proceedings of the 2021 International Symposium on Medical Robotics (ISMR), Atlanta, GA, USA, 17–19 November 2021; pp. 1–7.
25. Kreyszig, E. *Advanced Engineering Mathematics*, 10th ed.; John Wiley & Sons: Hoboken, NJ, USA, 2006.
26. O'Sullivan, L.W.; Gallwey, T.J. Upper-Limb Surface Electromyography at Maximum Supination and Pronation Torques: The Effect of Elbow and Forearm Angle. *J. Electromyogr. Kinesiol.* **2002**, *12*, 275–285. [CrossRef]
27. Matsuoka, J.; Berger, R.A.; Berglund, L.J.; An, K.N. An Analysis of Symmetry of Torque Strength of the Forearm Under Resisted Forearm Rotation in Normal Subjects. *J. Hand Surg.* **2006**, *31*, 801–805. [CrossRef] [PubMed]
28. Cimatti, B.; Marcolino, A.M.; Barbosa, R.I.; Fonseca, M.D.C.R. A Study to Compare Two Goniometric Methods for Measuring Active Pronation and Supination Range of Motion. *Hand Ther.* **2013**, *18*, 57–63. [CrossRef]
29. Soucie, J.M.; Wang, C.; Forsyth, A.; Funk, S.; Denny, M.; Roach, K.E.; Boone, D. Range of Motion Measurements: Reference Values and a Database for Comparison Studies. *Haemophilia* **2011**, *17*, 500–507. [CrossRef]
30. Rahman, H.A.; Fai, Y.C.; Ming, E.S.L. Analysis of Human Hand Kinematics: Forearm Pronation and Supination. *J. Med. Imaging Health Inform.* **2014**, *4*, 245–249. [CrossRef]
31. Morrey, B.F.; Askew, L.J.; Chao, E.Y. A Biomechanical Study of Normal Functional Elbow Motion. *J. Bone Jt. Surg.* **1981**, *63*, 872. [CrossRef]
32. Sardelli, M.; Tashjian, R.Z.; MacWilliams, B.A. Functional Elbow Range of Motion for Contemporary Tasks. *J. Bone Jt. Surg.* **2011**, *93*, 471. [CrossRef] [PubMed]
33. Realmuto, J.; Sanger, T. A robotic forearm orthosis using soft fabric-based helical actuators. In Proceedings of the 2019 2nd IEEE International Conference on Soft Robotics (RoboSoft), Seoul, Republic of Korea, 14–18 April 2019; pp. 591–596.
34. Bartlett, N.W.; Lyau, V.; Raiford, W.A.; Holland, D.; Gafford, J.B.; Ellis, T.D.; Walsh, C.J. A Soft Robotic Orthosis for Wrist Rehabilitation. *J. Med. Devices* **2015**, *9*, 030918. [CrossRef]
35. Trotobas, C. Restauration des Fonctions des Membres Supérieurs par des Orthèses d'Assistance pour des Personnes Ayant une Paralysie. Ph.D. Thesis, Université de Montpellier, Montpellier, France, 2023.

Disclaimer/Publisher's Note: The statements, opinions and data contained in all publications are solely those of the individual author(s) and contributor(s) and not of MDPI and/or the editor(s). MDPI and/or the editor(s) disclaim responsibility for any injury to people or property resulting from any ideas, methods, instructions or products referred to in the content.